Journal of Sound and Vibration (2002) **257**(1), 131–156
doi:10.1006/jsvi.5035, available online at http://www.idealibrary.com on IDEAL®

PREDICTION OF NON-CAVITATING UNDERWATER PROPELLER NOISE

H. Seol

School of Mechanical and Aerospace Engineering, BD 136-1318, *Seoul National University, Seoul* 151-742, *South Korea. E-mail: hsseol7@snu.ac.kr*

B. Jung

School of Mechanical and Aerospace Engineering, Seoul National University, Seoul 151-742, *South Korea*

J.-C. Suh

Department of Naval Architecture and Ocean Engineering, BD 42, *Seoul National University, Seoul* 151-742, *South Korea*

AND

S. Lee

School of Mechanical and Aerospace Engineering, BD 301-1303, *Seoul National University, San* 56-1 *Seoul* 151-742, *Shilim-Dong Kwanak-Gu, South Korea. E-mail: solee@plaza.snu.ac.kr*

(*Received* 10 *May* 2001, *and in final form* 2 *January* 2002)

Non-cavitation noise of underwater propeller is numerically investigated. The main purpose is to analyze non-cavitation noise in various operating conditions with different configurations. The noise is predicted using time-domain acoustic analogy and boundary element method. The flow field is analyzed with potential-based panel method, and then the time-dependent pressure data are used as the input for Ffowcs Williams–Hawkings formulation to predict the farfield acoustics. Boundary integral equation method is also considered to investigate the effect of ducted propeller. Sound deflection and scattering effect on the duct is considered with the BEM. The governing equations are based on the assumption that all acoustic pressure is linear. A scattering approach is applied in which the acoustic pressure field is split into the known incident component and the unknown scattered component. Noise prediction results are presented for single propeller and ducted propeller in non-uniform flow conditions similar to real situation. The investigation reveals that the effect of a duct on the acoustic performance propeller is small in the far field under non-cavitating situations since the noise directivities of single and ducted propellers are almost the same. Only the high order BPFs are influenced by the existence of the duct.

1. INTRODUCTION

Sound generated by a propeller is critical in underwater detection, and is often related to the survivability of the vessels especially for military purposes. Marine propeller noise can be classified into cavitating and non-cavitating noise. Cavitation of the marine propeller is the most prevalent source of underwater sound in oceans and is often the dominant noise source of a single marine vehicle. However, submarines and torpedoes are usually operated deep enough under the sea to avoid cavitation [1]. Compared with the extensive amount of

0022-460X/02/$35.00

literatures concerning cavitation noise of propellers, works concerning the non-cavitation noise of propellers are hard to find.

The non-cavitation noise of underwater propeller is numerically investigated in this study. Potential-based panel method is coupled with acoustic analogy and boundary element method in analyzing the non-cavitating noise. A brief description of the flow analysis tool is given along with verification. The panel method developed by the authors is an embodiment of the classical Green third identity for velocity potential with the Kutta condition to ensure the uniqueness. Noise prediction is performed using time-domain acoustic analogy. Blade surfaces are divided into rectangular panels radiating noise at different retarded times. The flow solver employs hyperboloidal panel elements on the exact surfaces of the propeller blades, containing all the complications of skew, rake and pitch changes found in most marine propellers. With the improved Kutta condition, the panel method proves to be robust and accurate.

There are various ways to evaluate Ffowcs Williams–Hawkings equation and the three types of noise source terms (monopole, dipole, and quadrupole) proposed [2]. Farrasat proposed a time-domain formulation that can predict noise from an arbitrarily shaped object in motion without the numerical differentiation of the observer time [3, 4]. The implementation of this formulation is quite straightforward because contributions from each panel with different retarded times are added to form an acoustic wave. The quadrupole noise source term is neglected in this study since the rotating speed of the propeller is much lower than the underwater speed of sound. In addition, the sound deflection and scattering effect on the duct is simulated with the boundary integral element method.

The purpose of this research is to analyze non-cavitation noise from underwater propellers in various operating conditions with different configurations. A propeller in a uniform flow condition produces both monopole thickness noise and dipole Gutin noise [1]. It is known, however, that Gutin noise is negligible for underwater propellers [5]. Under non-uniform inflow conditions, propellers produce dipole noise due to the unsteady loading on blade surfaces. To assess the effect of duct on the generated noise, a ducted propeller is also analyzed. Through these studies, the dominant noise source of marine propellers is analyzed, which will provide a basis for proper noise control strategies under non-cavitating conditions.

2. METHODOLOGY

2.1. FLOW SOLVER

The fundamentals of panel method are described by Kerwin and co-workers [6, 7], so only a brief description is given here. The method is based on the Green's third identity for velocity potential ϕ.

$$2\pi\phi = \int_S \phi \frac{\partial G}{\partial n}\,\mathrm{d}S + \int_{S_w} \Delta\phi \frac{\partial G}{\partial n}\,\mathrm{d}S. \tag{1}$$

Here, the body surface S is composed of propeller blade surface S_B, hub surface S_H and duct surface S_D (only for ducted propellers). The wake surface S_W is composed of propeller wake surface S_{BW} and duct wake surface S_{DW} (only for ducted propellers).

The surfaces and wakes of propeller and duct are discretized into hyperboloidal panels, where dipoles and sources of constant strength are distributed. The Kutta condition [8] is used and the pressure equality at the trailing edge of the blade and duct is also enforced.

Equation (1) yields a unique solution using the Kutta condition. The velocities on the boundary surfaces are obtained by differentiating the resulting velocity potential. Once the velocities are found, the pressure distribution is calculated from Bernoulli's equation. Since the co-ordinate system is fixed on the propeller in this research, the pressure on the propeller blade P_B is obtained by the following equation:

$$P_B = P_\infty - \rho \mathbf{V} \cdot \nabla\phi - \tfrac{1}{2}\rho(\nabla\phi)^2, \tag{2}$$

where $\mathbf{V}$ is undisturbed inflow velocity vector observed in the moving co-ordinate system fixed to propeller axis.

Furthermore, the potential on the duct changes with the angular location of the blade as the propeller blade rotates. This change is written as follows by the chain rule:

$$\frac{\partial\phi}{\partial t} = \omega \frac{\partial\phi}{\partial\theta} = 2\pi n \frac{\partial\phi}{\partial\theta}.$$

Adding the above term to equation (2), the pressure on the duct P_D is defined as follows:

$$P_D = P_\infty - 2\pi\rho n \frac{\partial\phi}{\partial\theta} - \rho \mathbf{V} \cdot \nabla\phi - \tfrac{1}{2}\rho(\nabla\phi)^2. \tag{3}$$

Panel method for solving the unsteady propeller problem was developed by Hsin [9–11]. This method is based on a discrete time-stepping algorithm. The integral equation (1) is solved at each time step and the time-dependent terms of equation (1) are updated for the next time step. The duct effect is also included for a ducted propeller. The discretized form of equation (1) is as follows [14, 15]:

$$\sum_{j=1}^{N_P} a_{i,j}\phi_j(n) + \sum_{m=1}^{M_B+M_D} W_{i,m,1}\Delta\phi_{m,1}(n) = RHS_i(n), \qquad i = 1, 2, \ldots, N_P, \tag{4}$$

$$RHS_i(n) = \sum_{K=1}^{N_B}\sum_{j=1}^{N_P} b_{i,j}^K \sigma_j^K(n) - \sum_{K=2}^{N_B}\sum_{j=1}^{N_P} a_{i,j}^K \phi_j^K(n) - \sum_{K=2}^{N_B}\sum_{m=1}^{M_B+M_D}\sum_{l=1}^{N_W} W_{i,m,l}^K \Delta\phi_{m,l}^K(n) - \sum_{m=1}^{M_B+M_D}\sum_{l=2}^{N_W} W_{i,m,l}^K \Delta\phi_{m,l}(n).$$

Here, N_B is the number of blades. M_B and M_D are the number of panels in the radial direction on the blade and in the circumferential direction on the duct respectively. N_W is the number of panels along the streamwise direction of the blade and the duct wake. N_P is the total number of panels on blade, hub and duct.

2.2. ACOUSTIC PREDICTION

Noise prediction can be represented as the solution of the wave equation if the distribution of sources on the moving boundary (the blade surface) and in the flow field is known. Ffowcs Williams and Hawkings derived the governing differential equation by applying the acoustic analogy of Lighthill to bodies in motion. Ffowcs Williams and Hawkings formulated the following equation for the manifestation of acoustic analogy

proposed by Lighthill [12]:

$$\frac{1}{c_0^2}\frac{\partial^2 p'}{\partial t^2} - \nabla^2 p' = \frac{\partial}{\partial t}[\rho_0 v_n |\nabla f| \delta(f)] - \frac{\partial}{\partial x_i}[l_i |\nabla f| \delta(f)] - \frac{\partial^2}{\partial x_i \partial x_j}[T_{ij} H(f)]. \tag{5}$$

The three source terms on the right-hand side of equation (5) are the monopole, dipole and quadrupole terms. Here $f = 0$ describes the surface of the blade and $p'$is the acoustic pressure while ρ_0 and c_0 each represent the mean fluid density in an undisturbed medium and the acoustic wave velocity respectively. The term v_n is the local normal velocity of the blade surface, l_i is the force per unit area applied on the fluid and the non-linear shear stress T_{ij} is the Lighthill's tensor, $T_{ij} = \rho u_i u_j - \tau_{ij} + (p' - c_0^2 \rho')\delta_{ij}$. Farrasat neglects the volume source term, or quadrupole term, in the Ffowcs Williams and Hawkings equation on the evident basis that the term becomes important only for strongly transonic flow and this quadrupole source strength is generally negligible in practice [4, 13]. So T_{ij} can be neglected since only low-speed propellers are considered in this work. The quantity $l_i$can also be denoted as $p_{ij}\hat{n}_j$, where p_{ij} is the compressible stress tensor including the surface pressure and the viscous stress. The term $\hat{n}_j$ is the surface normal pointing outward from $f = 0$ and the Dirac delta and the Heaviside functions are written as $\delta(f)$ and $\mathrm{H}(f)$ respectively.

The solution for the acoustic pressure can be obtained in the following form by using the Green function and co-ordinate transformations.

$$4\pi p'(\mathbf{x}, t) = \frac{1}{c_0}\frac{\partial}{\partial t}\int_{f=0}\left[\frac{\rho_0 c_0 v_n + l_r}{r(1 - M_r)}\right]_{ret} \mathrm{d}S + \int_{f=0}\left[\frac{l_r}{r^2(1 - M_r)}\right]_{ret} \mathrm{d}S \tag{6}$$

where l_r and M_r are the forces on the fluid per unit area and Mach number in the radiation direction respectively. The subscript *ret* denotes that the integrand is evaluated at the retarded time. The speed and accuracy of the numerical calculation are improved by eliminating the numerical differentiation; therefore using $g = \tau - t + r/c_0$ and the fact that r is a function of τ gives

$$\left.\frac{\partial}{\partial t}\right|_{\mathbf{x}} = \left(\frac{1}{1 - M_r}\left.\frac{\partial}{\partial \tau}\right|_{\mathbf{x}}\right)_{ret}.$$

This relation allows the time derivation to be taken inside the first integral.

Then from using the relations,

$$\frac{\partial r}{\partial \tau} = -v_r,$$

$$\frac{\partial \hat{r}_i}{\partial \tau} = \frac{\hat{r}_i v_r - v_i}{r},$$

$$\frac{\partial M_r}{\partial \tau} = \frac{1}{c_o r}\left(r_i \frac{\partial v_i}{\partial \tau} + v_r^2 - v^2\right),$$

$$\frac{\partial v_n}{\partial \tau} = \left(\frac{\partial v_i}{\partial \tau}\hat{n}_i + v_i \frac{\partial \hat{n}_i}{\partial \tau}\right) \equiv \dot{v}_n.$$

The final result is as follows [4, 13]:

$$p'(\mathbf{x}, t) = p'_T(\mathbf{x}, t) + p'_L(\mathbf{x}, t), \tag{7}$$

where

$$4\pi p'_T(\mathbf{x}, t) = \int_{f=0}\left[\frac{\rho_0 \dot{v}_n}{r(1 - M_r)^2}\right]_{ret} \mathrm{d}S + \int_{f=0}\left[\frac{\rho_0 v_n (r\dot{M}_i \hat{r}_i + c_0 M_r - c_0 M^2)}{r^2(1 - M_r)^3}\right]_{ret} \mathrm{d}S$$

and

$$4\pi p'_L(\mathbf{x},t) = \frac{1}{c_0}\int_{f=0}\left[\frac{\dot{l}_i\hat{r}_i}{r(1-M_r)^2}\right]_{ret}\mathrm{d}S + \int_{f=0}\left[\frac{l_r - l_iM_i}{r^2(1-M_r)^2}\right]_{ret}\mathrm{d}S$$
$$+\frac{1}{c_0}\int_{f=0}\left[\frac{l_r(r\dot{M}_i\hat{r}_i + c_0M_r - c_0M^2)}{r^2(1-M_r)^3}\right]_{ret}\mathrm{d}S.$$

Here p'_T and p'_L, respectively, denote the acoustic pressure due to thickness and loading, corresponding to the monopole and the dipole terms. The dots on $\dot{M}_i$, $\dot{l}_i$ and $\dot{v}_n$ indicate the rate of variation with respect to retarded time. The above equation is valid for arbitrary blade motion and geometry. Near field and far field terms are seen explicitly as $1/r^2$ and $1/r$ terms in the integrals, respectively.

2.3. BOUNDARY ELEMENT METHOD

Ducted propeller noise is considered using a boundary element method. BEM is based on the equations of linearized acoustics and predicts the sound scattered by a finite length cylindrical duct that has been irradiated by some simple source process. Simple acoustic sources are used to generate incident sound. Source configurations are composed of N symmetrically spaced point sources and are situated on a disc perpendicular to the duct axis.

The scattering of sound by real duct configuration (JD-75) is considered. The duct is irradiated by incident sound produced by a collection of N point dipoles generated by unsteady loading on propeller blades. Acoustic propagation and radiation are based on the assumption of linearity. In this research, integral equations are derived through the application of the Green second theorem and through analysis of noise directivity according to the characteristic wave number.

2.3.1. *Governing equation and boundary condition*

The total acoustic pressure in the sound field is split into the known incident part and the unknown scattered part:

$$p'_t(r,\psi,z,t) = p'_i(r,\psi,z,t) + p'_s(r,\psi,z,t). \tag{8}$$

In regions of space and time that contain no scattering surfaces, $p'_s$is governed by the homogeneous wave equation:

$$\left[\frac{\partial^2}{\partial t^2} - \frac{1}{r}\frac{\partial}{\partial r}\left(r\frac{\partial}{\partial r}\right) - \frac{1}{r^2}\frac{\partial^2}{\partial\psi^2} - \frac{\partial^2}{\partial z^2}\right]p'_s = 0. \tag{9}$$

Acoustic pressure and radial velocity are related through the radial component of the acoustic momentum equation:

$$\frac{\partial u'_r}{\partial t} + \frac{\partial p'}{\partial r} = 0. \tag{10}$$

In a frame of reference moving with the duct, the symmetry of the source process is such that all dependent acoustic variables can be expressed as linear superposition of time harmonic circumferential modes:

$$p'_t(r,\psi,Z,t) = \sum_{n=-\infty}^{\infty} P_t^n(r,Z)\mathrm{e}^{\mathrm{i}(kt - nN\psi)} \tag{11a}$$

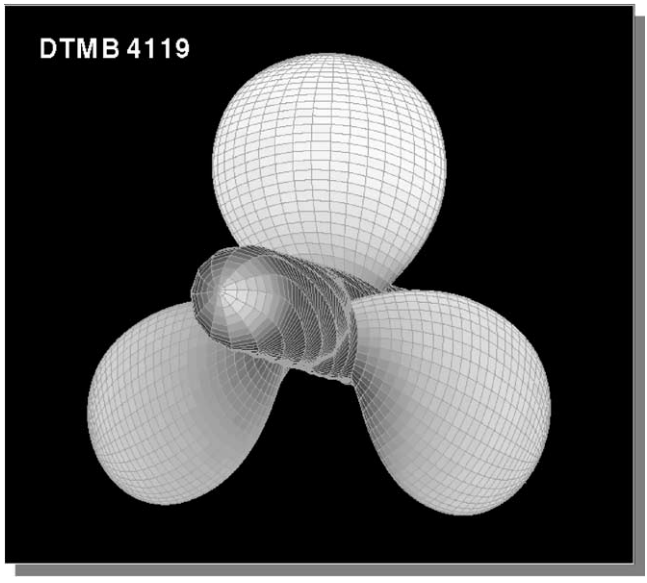

Figure 1. Single propeller model and condition. DTMB4119 with three blades, Rev: 120 r.p.m. forward speed: 1·6 m/s.

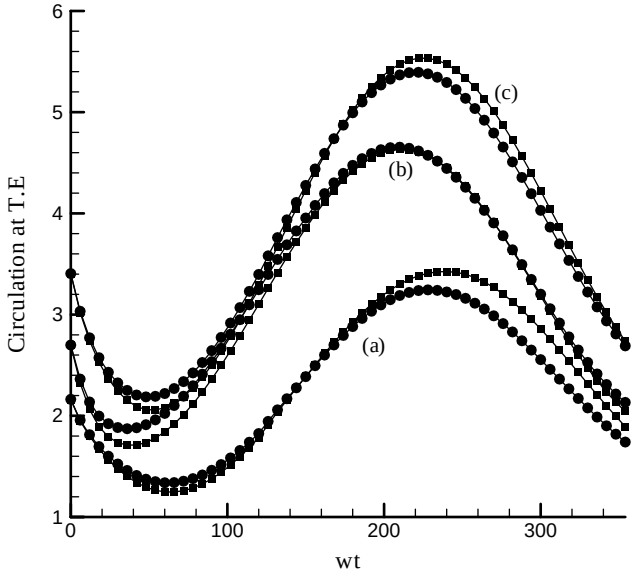

Figure 2. Comparison with other numerical methods. (circulation at trailing edge): (a) $r/R = 0{\cdot}2940$; (b) $r/R = 0{\cdot}5960$; and (c) $r/R = 0{\cdot}8278$. —●—, Present method; —■—, Hsin's method.

$$p_i'(r,\psi,Z,t) = \sum_{n=-\infty}^{\infty} P_i^n(r,Z)\mathrm{e}^{\mathrm{i}(kt-nN\psi)} \tag{11b}$$

$$p_s'(r,\psi,Z,t) = \sum_{n=-\infty}^{\infty} P_s^n(r,Z)\mathrm{e}^{\mathrm{i}(kt-nN\psi)} \tag{11c}$$

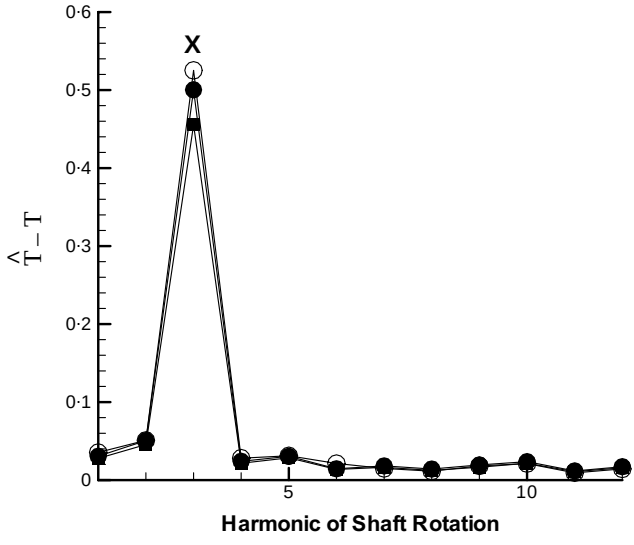

Figure 3. Thrust coefficient comparison with other numerical methods and experiments: ■, experiment; ○, without viscosity; ●, with viscosity; ×, Hsin's method.

and the radial component of total acoustic velocity is written as follows:

$$u_r'(r, \psi, Z, t) = \sum_{n=-\infty}^{\infty} U_r^m(r, Z) e^{i(kt - nN\psi)}. \tag{12}$$

Here, the stretched, moving axial co-ordinate Z is given by

$$Z = \frac{z - Mt}{\beta}. \tag{13}$$

For notational convenience, we define the circumferential mode number m and simplify the governing equations by new dependent variables Q, Q_s, Q_i, and V_r by the relations

$$Q(r, Z) = P(r, Z) e^{i\kappa MZ}, \tag{14a}$$

$$Q_i(r, Z) = P_i(r, Z) e^{i\kappa MZ}, \tag{14b}$$

$$Q_s(r, Z) = P_s(r, Z) e^{i\kappa MZ}, \tag{14c}$$

$$V_r(r, Z) = U_r(r, Z) e^{i\kappa MZ}. \tag{14d}$$

Combining equations (12–14) with equation (9) results in the two-dimensional Helmholtz equation for the mth modal coefficient of scattered pressure:

$$\left[\frac{1}{r}\frac{\partial}{\partial r}\left(r\frac{\partial}{\partial r}\right) + \frac{\partial^2}{\partial Z^2} - \frac{m^2}{r^2} + \kappa^2\right] Q_s = 0. \tag{15}$$

The momentum equation (10) can be written as

$$e^{-i(\kappa/M)Z} V_r(r, Z) = \frac{\beta}{M}\int_{-\infty}^{Z} e^{-i(\kappa/M)Z'} \frac{\partial Q}{\partial r}(r, Z')\, dZ'. \tag{16}$$

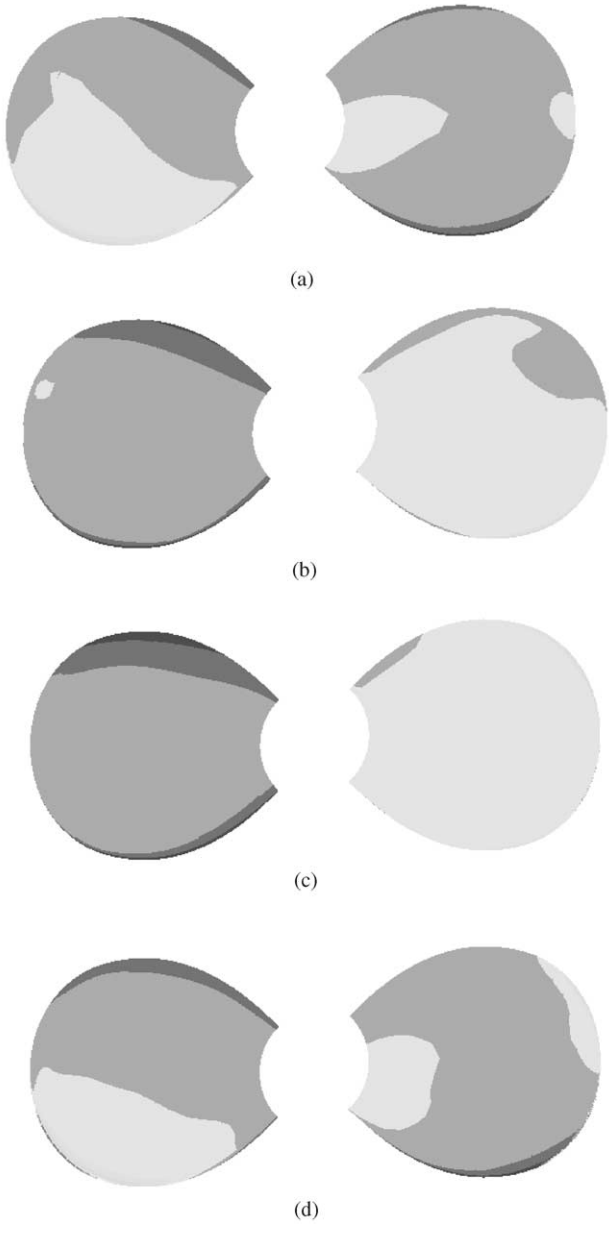

Figure 4. Blade suction and pressure surface pressure contour: (a) 0°; (b) 90°; (c) 180°; and (d) 270°.

Since a duct is stationary, we reduce it to

$$\left[\frac{1}{r}\frac{\partial}{\partial r}\left(r\frac{\partial}{\partial r}\right)+\frac{\partial^2}{\partial z^2}-\frac{m^2}{r^2}+k^2\right]P_s=0, \tag{17}$$

$$U_r(r,z)+\frac{i}{k}\frac{\partial P}{\partial r}(r,Z). \tag{18}$$

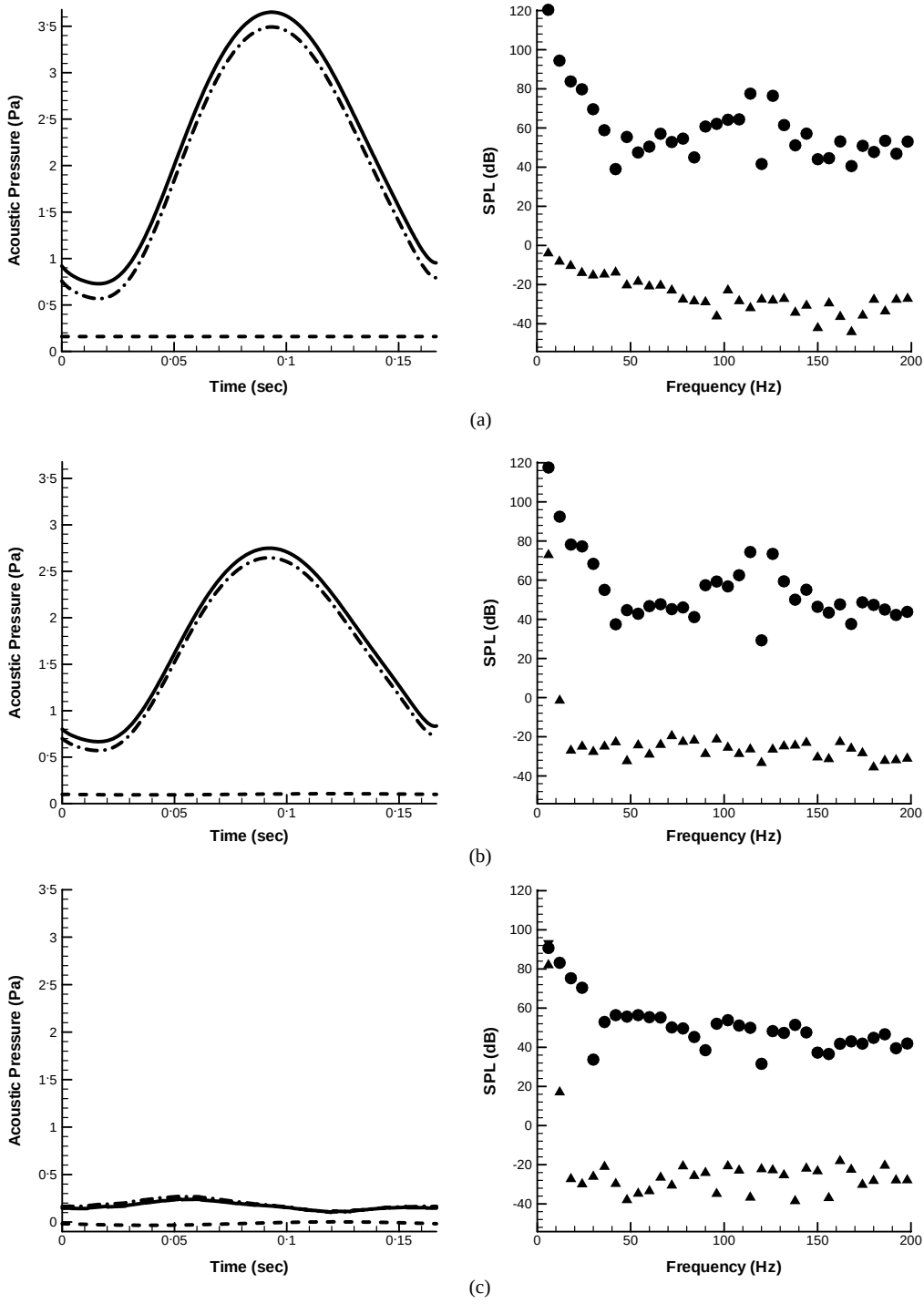

Figure 5. Acoustic pressure time histories and noise spectra of single propeller non-uniform flow: (a) $\theta = 0^\circ$, $d = 10R$; (b) $\theta = 45^\circ$, $d = 10R$; and (c) $\theta = 90^\circ$, $d = 10R$. ·····, thickness noise; —·—·, loading noise; ——, overall noise; ▼, thickness noise; ▲, loading noise; ●, overall noise.

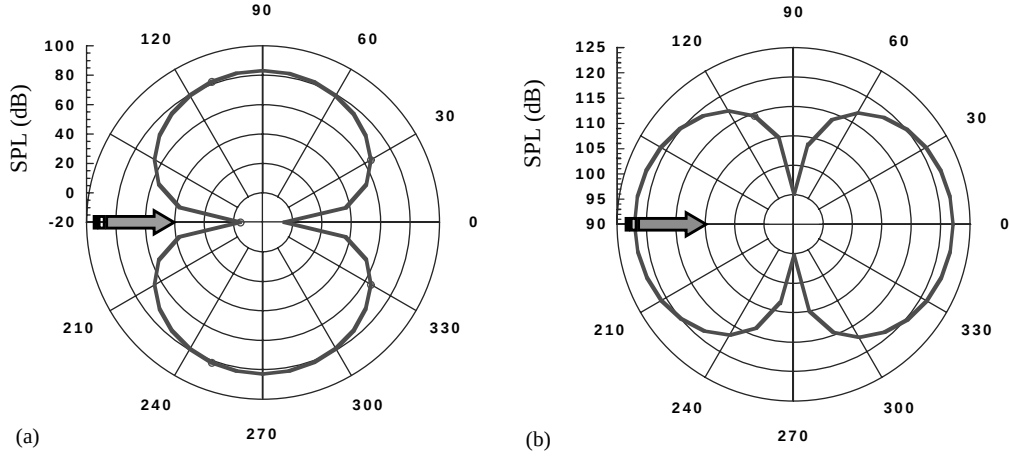

Figure 6. Single propeller non-uniform inflow for each noise directivity at distance $10R$: (a) thickness noise directivity; and (b) loading noise directivity.

As submarines and torpedoes do not use liner, hardwall boundary condition is used for the duct surface wall.

In order to obtain a unique solution, the behavior of the acoustic pressure in the far field and at the duct edge must be constrained. To ensure continuity of the trailing edge, the Kutta condition is imposed:

$$\lim_{Z \to a^+} [Q^+(Z) - Q^-(Z)] = 0. \tag{19}$$

For physically reasonable solution to exist, the Sommerfeld farfield radiation condition is imposed:

$$\lim_{\rho = \sqrt{r^2 + Z^2} \to \infty} \sqrt{\rho} \left(\frac{\partial Q}{\partial \rho} + \mathrm{i}\kappa Q \right) = 0. \tag{20}$$

2.3.2. *Helmholtz integral*

Helmholtz equation is computed for predicting the ducted propeller sound field. Boundary integral element method is used for solving the Helmholtz equation:

Helmholtz equation is expressed as follows.

$$\nabla^2 \phi(\mathbf{x}) + k^2 \phi(\mathbf{x}) = 0. \tag{21}$$

The sound pressure is related to the velocity potential by the formula

$$p(\mathbf{x}) = \mathrm{i}\rho\omega\phi(\mathbf{x}). \tag{22}$$

We now turn to the discrete form of the integral operators L_k, M_k, M_k^t and N_k that arises in the application of collocation to integral equation formulation of the Helmholtz equation.

To facilitate calculation, the Helmholtz integral operators are defined as follows [16]:

$$\{L_k \eta\}_\Gamma(\mathbf{p}, \mathbf{q}) \equiv \int_\Gamma G_k(\mathbf{p}, \mathbf{q}) \eta(\mathbf{q}) \, \mathrm{d}S_q, \tag{23a}$$

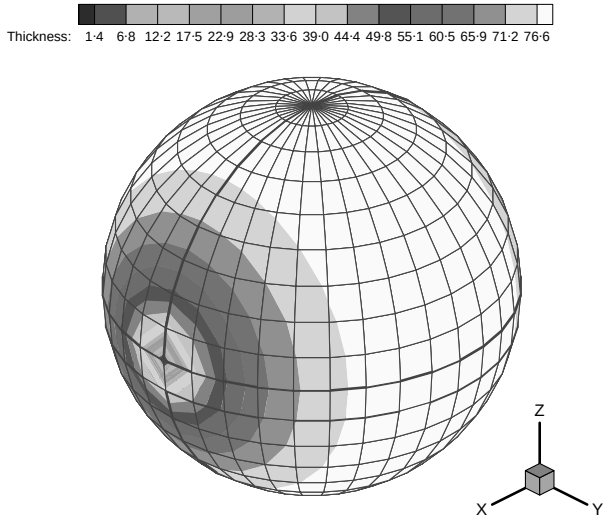

Figure 7. Single-propeller thickness noise and loading noise directivity three-dimensional contour: (a) thickness noise directivity; and (b) loading noise directivity.

$$\{M_k\eta\}_\Gamma(\mathbf{p},\mathbf{q}) \equiv \int_\Gamma \frac{\partial G_k(\mathbf{p},\mathbf{q})}{\partial \mathbf{n}_q}\,\eta(\mathbf{q})\,\mathrm{d}S_q, \tag{23b}$$

$$\{M_k^t\eta\}_\Gamma(\mathbf{p};\mathbf{u}_p) \equiv \frac{\partial}{\partial \mathbf{u}_p}\int_\Gamma G_k(\mathbf{p},\mathbf{q})\,\eta(\mathbf{q})\,\mathrm{d}S_q \tag{23c}$$

$$\{N_k\eta\}_\Gamma(\mathbf{p};\mathbf{u}_p) \equiv \frac{\partial}{\partial \mathbf{u}_p}\int_\Gamma \frac{\partial G_k(\mathbf{p},\mathbf{q})}{\partial \mathbf{n}_q}\,\eta(\mathbf{q})\,\mathrm{d}S_q, \tag{23d}$$

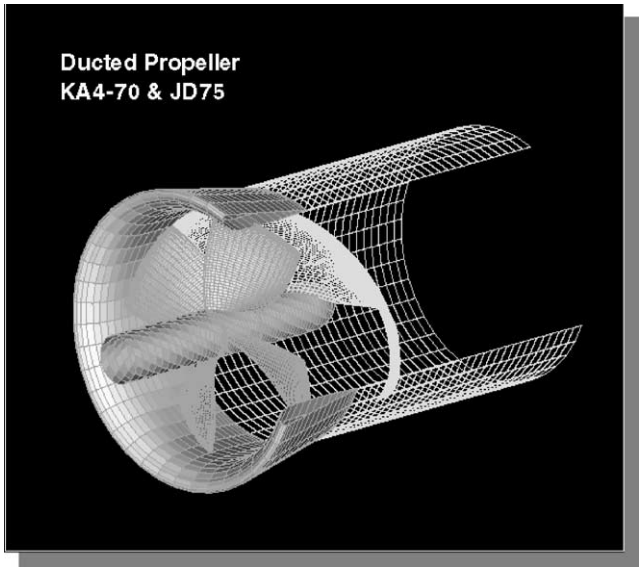

Figure 8. Ducted propeller model and condition. KA4-70 with four blades, Rev: 120 r.p.m., forward speed: 1·788 m/s.

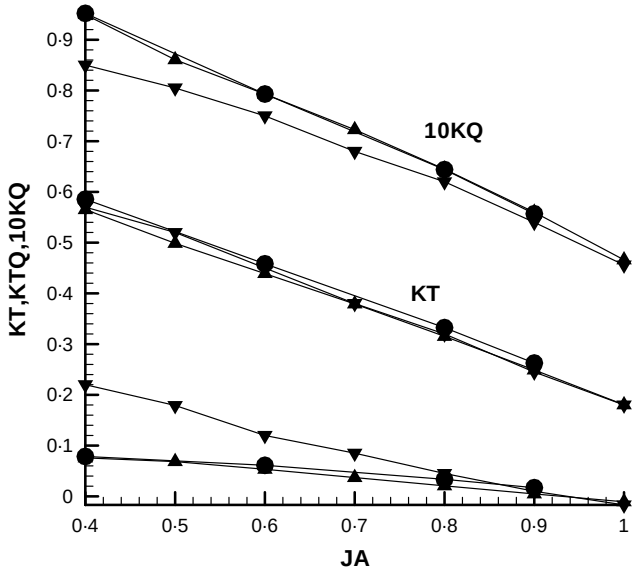

Figure 9. Comparison with experiment and uniform inflow result: —▲—, numerical result (steady); —▼—, numerical result (unsteady); —●—, experiment result.

where Γ is the boundary, n_q is the unique normal to Γ at q and $\eta(q)$ is a function defined for $q \in \Gamma$. $G_k(p, q)$ is the free-space Green function for the Helmholtz equation. In two-dimensional free space, the Green function is represented as follows:

$$G_k(\mathbf{p}, \mathbf{q}) = \frac{\mathrm{i}}{4} H_0^{(1)}(kr). \tag{24}$$

Here, $r = p - q$ and $H_0^{(1)}$ is the spherical Hankel function of the first kind of order zero.

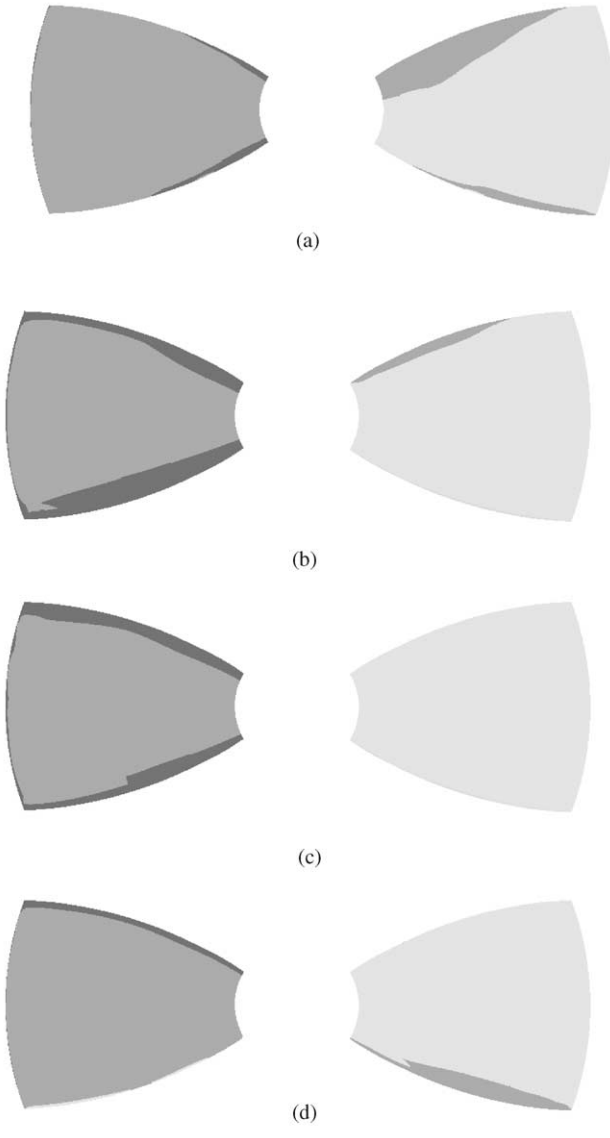

Figure 10. Blade suction and pressure surface pressure contour: (a) 0°; (b) 90°; (c) 180°; and (d) 270°.

The application of the Greens second theorem to the Helmholtz equation gives the following equations:

$$\{M_k\phi\}s(\mathbf{p}) - \phi(\mathbf{p}) = \{L_k v\}s(\mathbf{p}) \quad (p \in E), \tag{25a}$$

$$\{M_k\phi\}s(\mathbf{p}) - \tfrac{1}{2}\phi(\mathbf{p}) = \{L_k v\}s(\mathbf{p}) \quad (p \in S). \tag{25b}$$

ϕ and v are computed on the boundary from equation (25b), and the value of $\phi(p)$ for exterior points p in the domain can be obtained through equation (25a). The application of

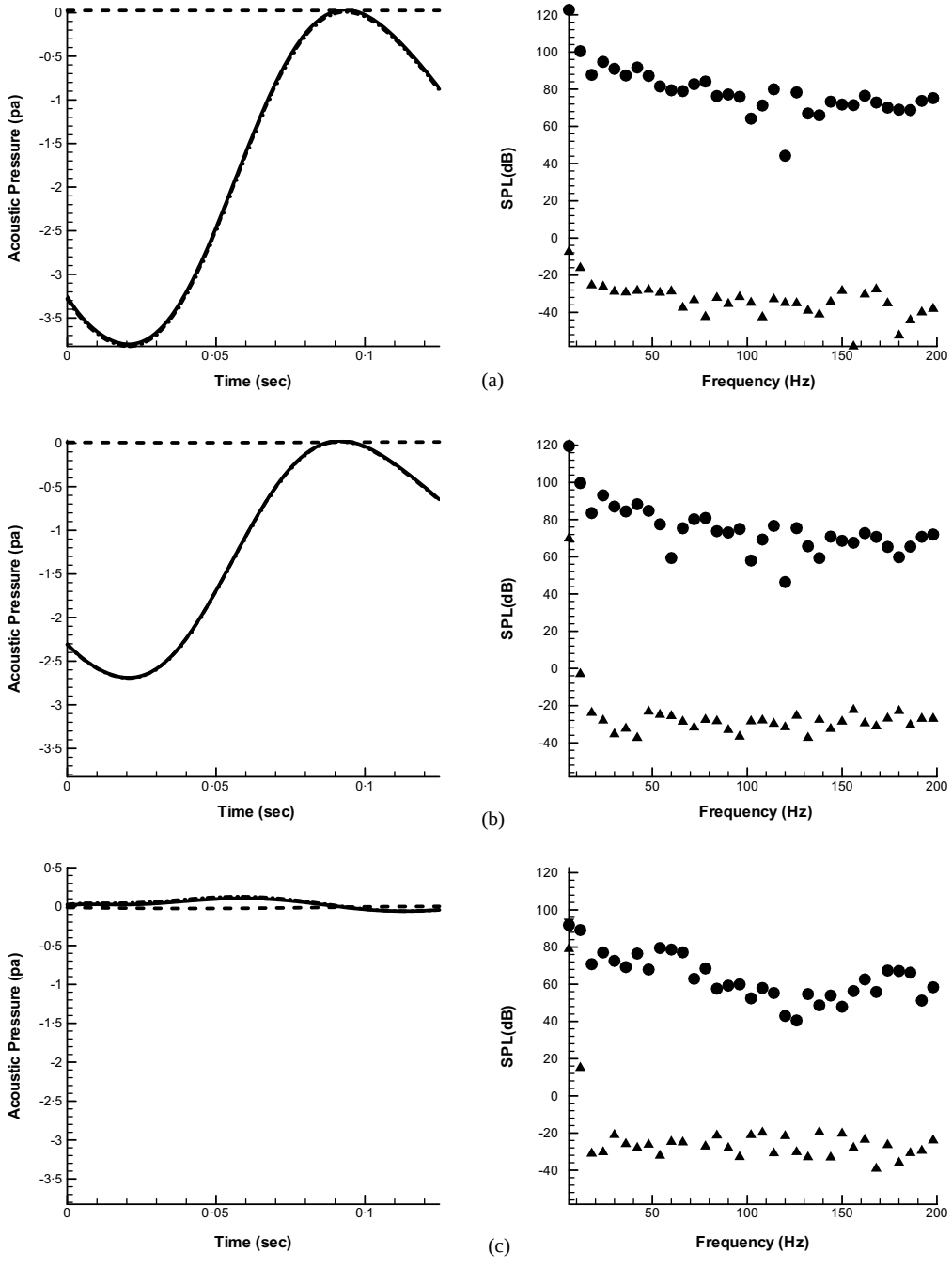

Figure 11. Acoustic pressure time histories and noise spectra of ducted propeller non-uniform flow: (a) $\theta = 0^\circ$, $d = 10R$; (b) $\theta = 45^\circ$, $d = 10R$; and (c) $\theta = 90^\circ$, $d = 10R$. $\cdots\cdots$, thickness noise; —·—·, loading noise; ——, overall noise; ▼, thickness noise; ▲, loading noise; ●, overall noise.

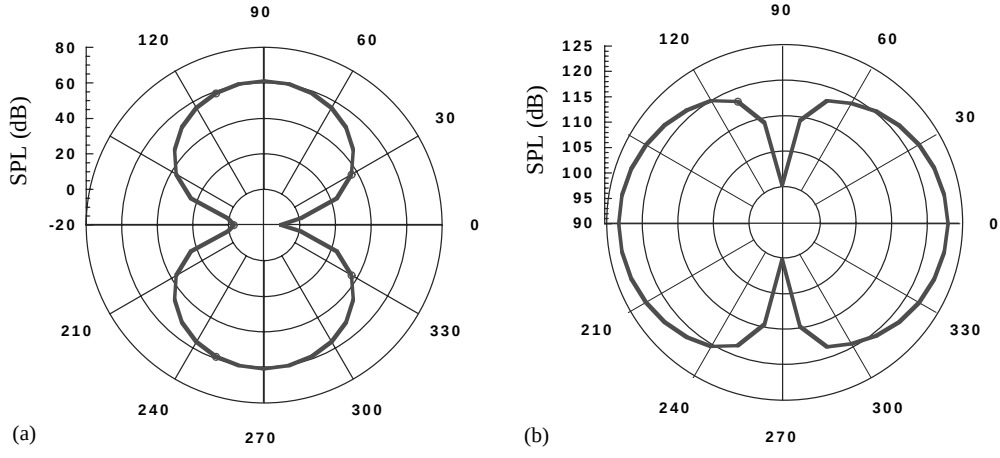

Figure 12. Ducted propeller non-uniform inflow for each noise directivity at distance $10R$: (a) thickness noise directivity; and (b) loading noise directivity.

collocation to integral equation (25b) reduces it to the following equation:

$$[\mathbf{M}_k - \tfrac{1}{2}\mathbf{I}]\underline{\hat{\phi}} = \mathbf{L}_k\underline{\hat{v}}. \tag{26}$$

The terms $\mathbf{L}_k$, $\mathbf{M}_k$ are $n \times n$ matrices arising from the discretization method. The components of L_k are defined by $[L_k]_{ij} = \{L_k\tilde{e}\}_{\Delta\tilde{S}_j}(p_i)$, where $\tilde{e}$ is the unit function.

The method, however, is singular at the characteristic wave number [17]. An improved direct formulation proposed by Burton and Miller [18] is thus used. The formulation is a hybrid of the elementary direct formulation (25b) and equation that arises through differentiating that equation with respect to the normal to the boundary:

$$\{N_k\phi\}s(\mathbf{p};\mathbf{n}_p) = \{(M_k^t + \tfrac{1}{2}I)v\}s(\mathbf{p};\mathbf{n}_p) \quad (\mathbf{p}\in S). \tag{27}$$

The improved direct integral equation formulation is simply a linear combination of equation (25) with this equation.

$$\{(M_k - \tfrac{1}{2}I + \mu N_k)\,\phi\}\, s(\mathbf{p};\mathbf{n}_p) = \{(L_k + \mu(M_k^t + \tfrac{1}{2}I))v\}\, s(\mathbf{p};\mathbf{n}_p) \quad (\mathbf{p}\in S). \tag{28}$$

The numerical solution of equation (28) gives both function of ϕ and v on the boundary and approximation of equation (25a) yields the solution at any point in the exterior.

3. RESULTS AND DISCUSSION

Basic flow fields of propellers with/without duct are obtained using potential-based panel method. In the case of a ducted propeller, the relative motion between the rotating propeller blades and the stationary duct requires that the influence of panels on the two different frames of reference be re-calculated at each time step.

In this section, both the flow field and the noise prediction results are presented for non-ducted/ducted propellers. The acoustic time history, noise spectra and noise directivity patterns of each noise source are analyzed.

The density and speed of sound in the undisturbed medium of standard water are 1026 kg/m^3 and 1500 m/s respectively. The reference pressure for calculating sound pressure level (SPL) is $1{\cdot}0 \times 10^{-6}$ Pa. The observer is located at the distance 10 times the propeller radius, R in the direction of $\theta = 0^\circ$, $\theta = 45^\circ$, $\theta = 90^\circ$ from the propeller shaft axis.

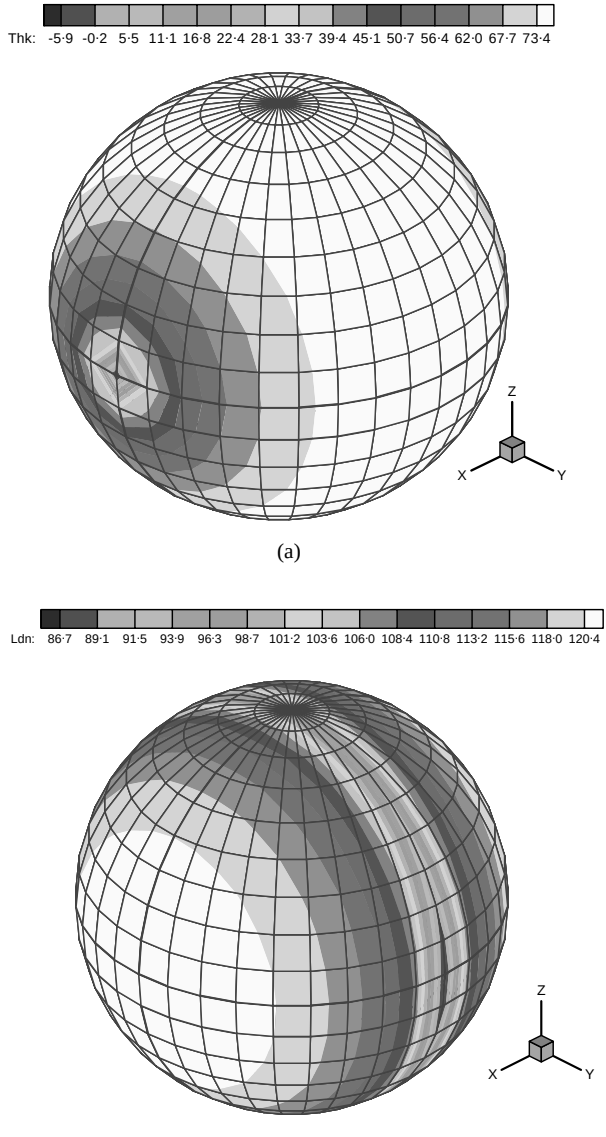

Figure 13. Ducted propeller thickness noise and loading noise directivity three-dimensional contour: (a) thickness noise directivity; and (b) loading noise directivity.

The observer positions are given in terms of the angle θ and the distance d. The axial angle θ is measured from the downstream propeller axis and the distance d is given in terms of the radius of the propeller R.

For ducted propellers, the sound deflection and scattering effect are predicted using the boundary integral equation method.

3.1. SINGLE PROPELLER IN A NON-UNIFORM FLOW

The propeller model having three blades (DTMB4119) is shown in Figure 1. The propeller is operated at 120 r.p.m. with a forward velocity of 1·6 m/s.

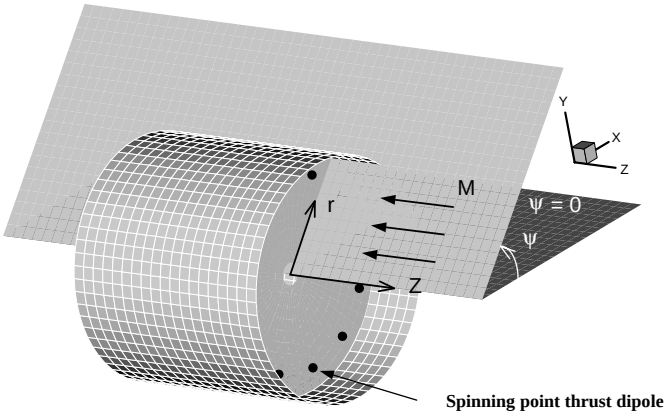

Figure 14. BEM Modelling.

Flow fields are computed using this propeller model in a non-uniform flow. Each propeller blade is modelled with 20 spanwise divisions and 40 chordwise divisions (20 for upper surface and 20 for lower surface) to fully consider the thickness of the blade. In order to validate the unsteady panel method, the results are compared with other numerical methods [9]. The comparison results are shown in Figure 2, which shows excellent agreement between the two methods.

The experimentally simulated three-cyclic wake is used to start a non-uniform inflow. Figure 3 shows the thrust variation coefficient comparison of the present method with other numerical methods and experiment. The blade surface pressure contours when the blade is located at 0, 90, 180, and 270° are shown in Figure 4.

The noise calculations are performed in various observer positions. The directivity of noise can also be analyzed through this method. The acoustic pressure time history and noise spectra calculated at various positions are shown in Figure 5. The directivity of the thickness noise is a simple 8-shaped curve with the maximum occurring on the propeller rotation plane. Monopole thickness noise, with its acoustic energy concentrated at its lower harmonics, is known to radiate strongest towards the plane of blade rotation. The unsteady loading noise is known to be dipole in nature, with a strong radiation tendency towards the observer on the hub axis. The results are depicted well in Figure 6, with the directivity of each noise source measure being at a distance of $10R$. The unsteady loading noise is mainly governed by irregularities—the fluctuation of surface pressure, while the thickness noise is dominated by the periodicity of propeller rotation. Since the noise prediction is highly affected by inflow conditions, the directivity of the noise generated by a propeller in a non-uniform flow is complex. Three-dimensional directivity contours are thus shown in Figure 7. The results show that the overall noise level is highest at the location of the hub center. The trend is a the characteristic of unsteady loading noise, and the monopole noise due to blade thickness is very small compared with the dipole noise. This is due to the fact that the propeller blades are not sufficiently thick enough to cause much volume displacement of the fluid.

3.2. DUCTED PROPELLER IN A NON-UNIFORM FLOW

For submarine propellers or torpedoes, ducts are used for propulsion efficiency and cavitation noise reduction. Ducts used in marine propellers are usually very short compared

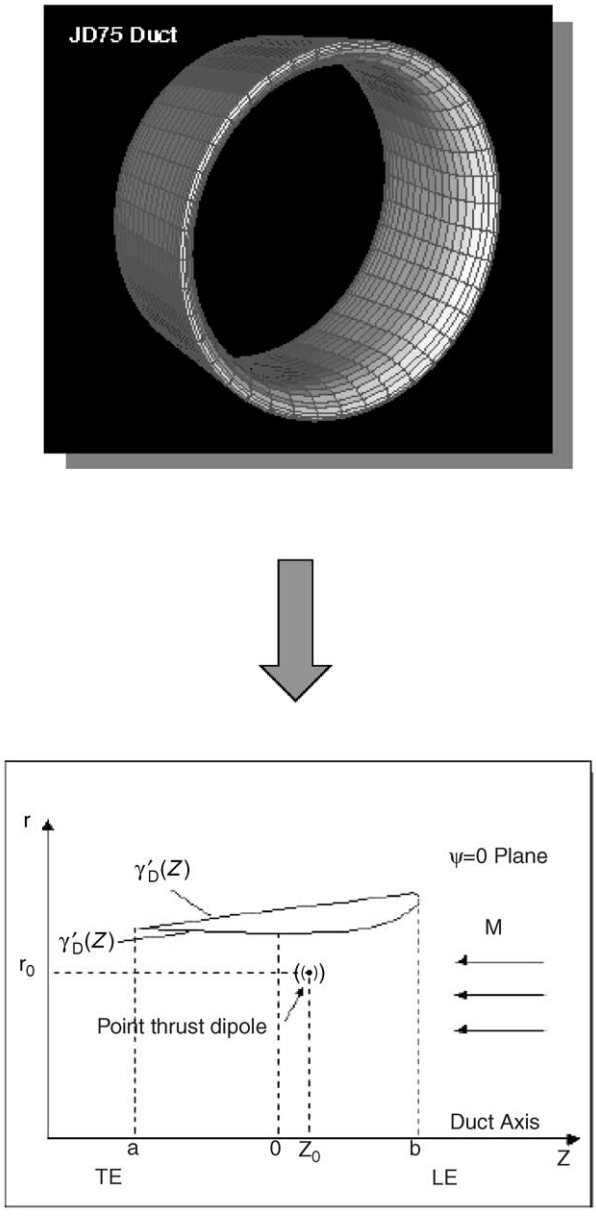

Figure 15. JD-75 duct and source modelling.

with the wavelength of non-cavitation noise produced by marine propellers. So diffraction, interference and the cut off of components below the cut-off frequency often found in duct acoustics can be neglected [19]. The noise prediction module is not affected as much as the flow analysis module when a duct is attached. The flow analysis module must be changed extensively due to the inclusion of a duct.

The flow solver is applied to a ducted propeller in a non-uniform flow. The propeller has four blades, and the pitch to diameter is 1·4. The blade outline is one of the Wageningen KA4-70. The JD75duct model is adopted. The gap between the propeller tip and the duct is

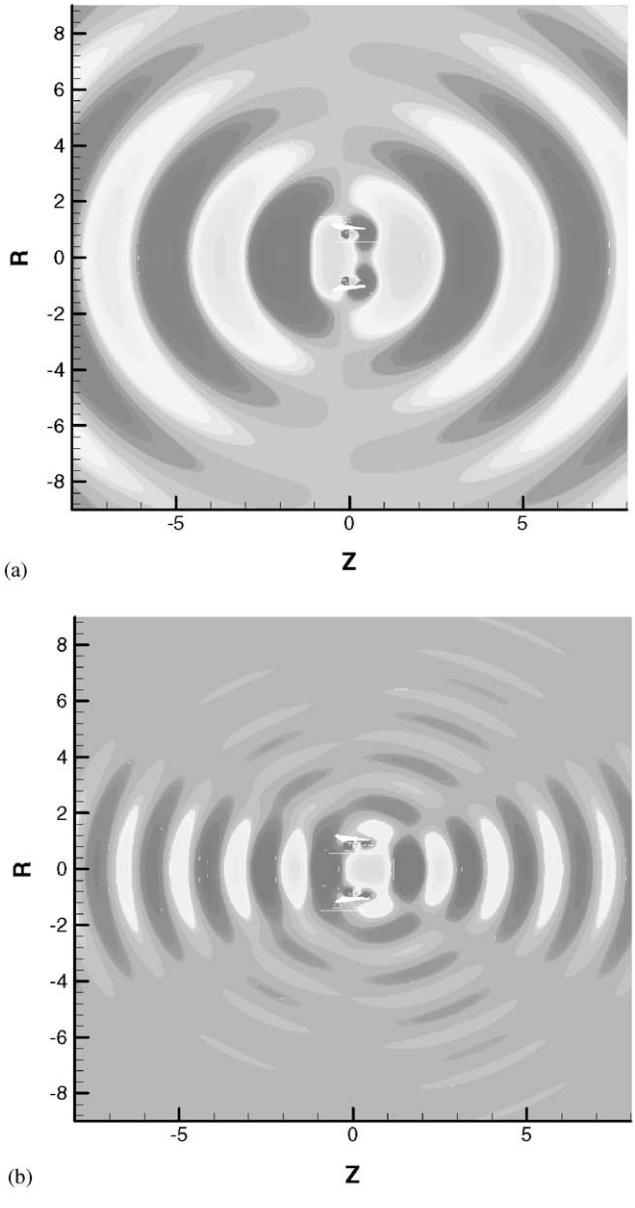

Figure 16-1. Acoustic pressure fields with respect to Helmholtz number: (a) $ka = 2$; and (b) $ka = 4$.

0·8% of the propeller radius. A typical panel arrangement for the calculation of the ducted propeller is shown in Figure 8. As mentioned earlier, the three-cyclic wake is used for the onset of the non-uniform inflow. To validate the unsteady panel method for a ducted propeller, calculations are performed with a uniform flow condition. As shown in Figure 9, the resulting open-water characteristics are similar to the results from the steady panel method in the uniform flow and experiment. The propeller blade surface pressure contours are shown in Figure 10. Figure 11 shows the acoustic pressure time histories and noise spectra at various observer positions in the non-uniform flow. The noise directivity shows a similar tendency with the non-ducted single propeller in the non-uniform flow. The

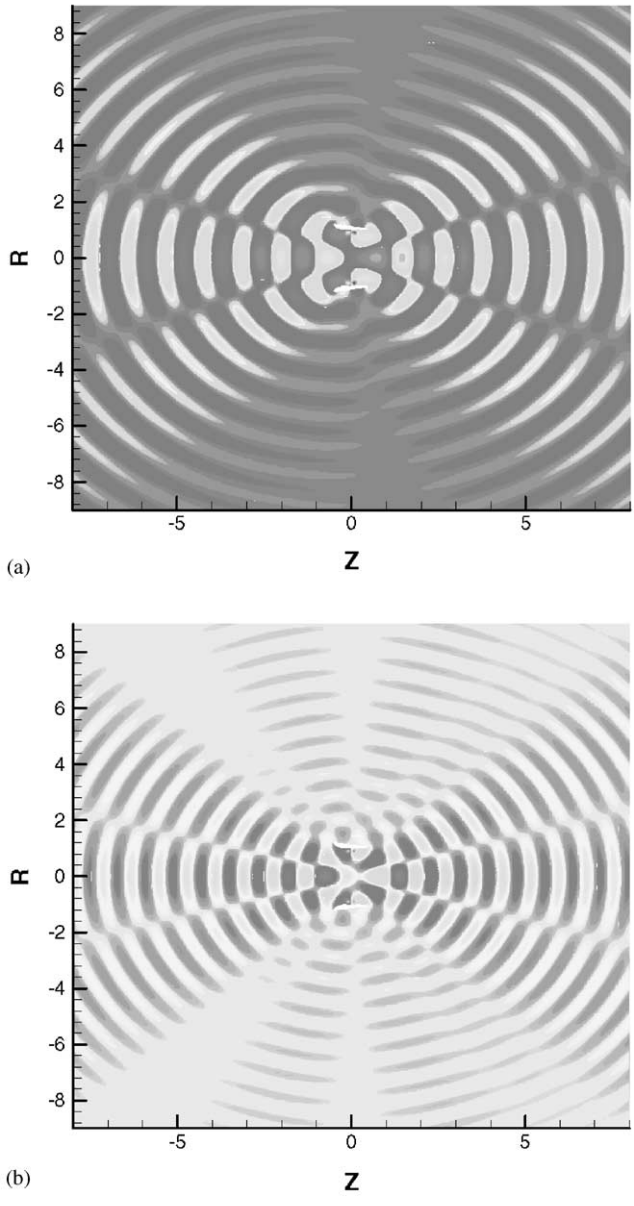

Figure 16-2. Acoustic pressure fields with respect to Helmholtz number: (a) $ka = 6$; and (b) $ka = 8$.

directivity of each noise component is plotted in Figure 12. The direction of maximum thickness noise is perpendicular to the propeller shaft axis as in the case of the non-ducted propeller. The noise directivity of unsteady loading noise of the ducted propeller is quite similar to that of a single propeller. The three dimensional noise directivity contours are shown in Figure 13.

In case of torpedoes and high-speed marine propellers with high blade passage frequency (BPF) noise, the acoustic waves exhibit relatively short wavelengths. For these cases, the duct effect cannot be neglected. Boundary element method is thus used to predict sound

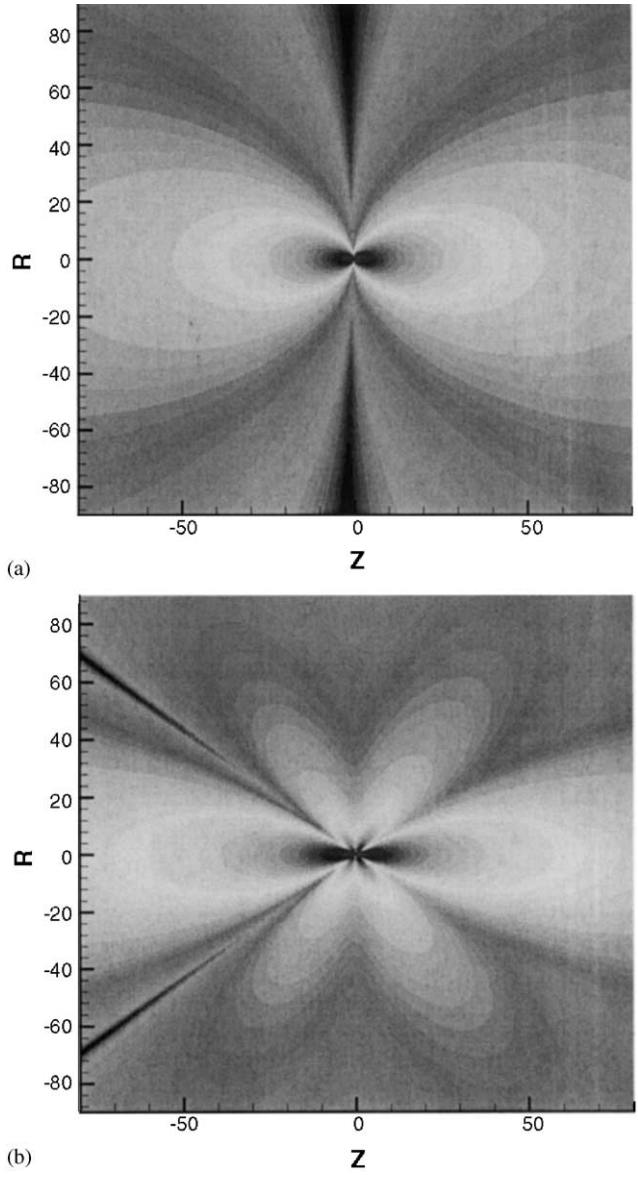

Figure 17-1. Sound pressure fields with respect to Helmholtz number: (a) $ka = 2$; and (b) $ka = 4$.

deflection and scattering. Four spinning point dipoles, located at $0{\cdot}9r_{max}$ are modelled. The configuration approximates the thrust component of loading noise produced by the 4-bladed propeller. The JD-75 duct configuration is used. The duct is divided into 38 boundary elements and the duct walls are modelled as hard. The model is illustrated in Figures 14 and 15.

Analysis is from the first order BPF to the third order harmonic. Acoustic pressure, sound pressure level and noise directivity are computed.

Figures 16 and 17 show the acoustic pressure field and the sound pressure level with respect to the helmholtz number. Noise directivity patterns are shown in Figure 18. As

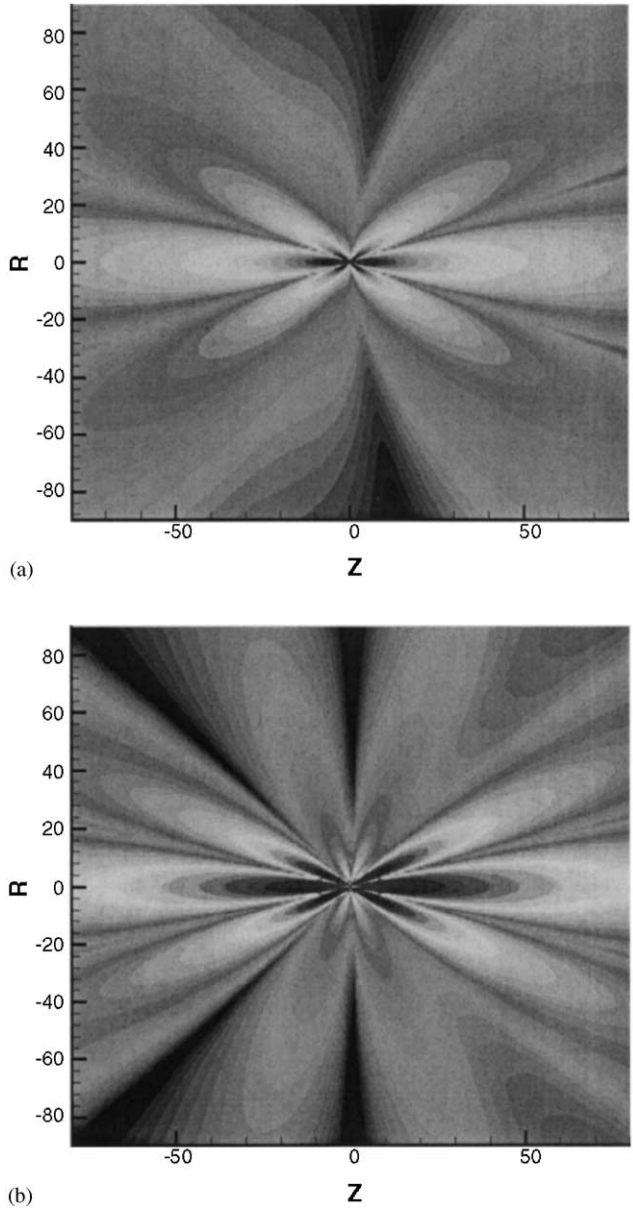

Figure 17-2. Sound pressure fields with respect to Helmholtz number: (a) $ka = 6$; and (b) $ka = 8$.

shown in these figures, the number of acoustic lobes increases with the order of the BPF. The noise direction angle and the axial mode number are shown in Table 1. In the first BPF ($ka = 2$), the noise directivity pattern is similar to the acoustic analogy results. But the noise directivity pattern is more complex in the higher order BPFs due to sound deflection and scattering by the duct. In general, the first BPF noise is seen to be dominant. The effect of a duct on noise propagation can therefore be stated to be small because of the long fundamental wavelength under non-cavitation condition. Duct does not affect the acoustic performance of a propeller in the far field under the non-cavitation situation.

TABLE 1

KA4-70 and JD 75 Duct propeller noise directivity

	Wave number	Axial mode number	Axial mode direction angle (deg)
1 BPF	2·0	1	0
2 BPF	4·0	2	60, 117
3 BPF	6·0	2	38, 143
4 BPF	8·0	3	30, 72, 107, 152

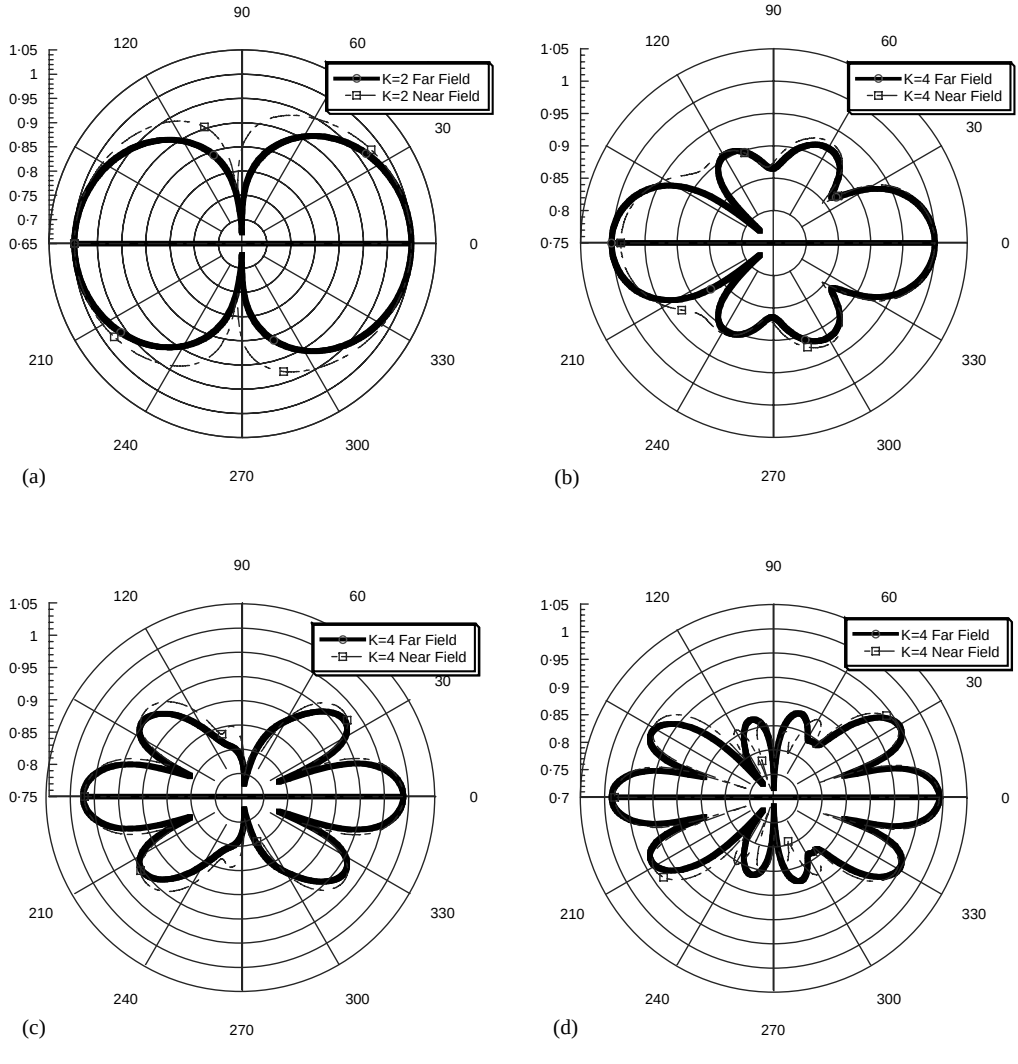

Figure 18. KA470 & JD 75 duct propeller noise directivity. (a) ka = 2; (b) ka = 4; (c) ka = 6; (d) ka = 8.

4. CONCLUSION

The non-cavitating noise generated by underwater propeller is analyzed numerically in this study. Potential-based panel method coupled with time-domain acoustic analogy is used to predict the noise generated by single and ducted propellers in a non-uniform flow condition.

The time-stepping potential-based flow solver is modified to increase the time resolution of the flow analysis and the results are compared with other numerical schemes and experiments. The flow solver is proved to be robust and accurate. For noise prediction, Ffowcs Williams–Hawkings equation is adopted in the form proposed by Farrasat.

In a non-uniform flow condition similar to the real situation, the noise directivity pattern is a direct result of the dipole dominating the overall noise level.

Sound deflection and scattering effect due to the duct is considered using the boundary element method. Acoustic pressure and noise directivity is analyzed according to wave number. The first BPF noise directivity is similar to that of the single propeller case. But in high order BPFs, when the wavelengths are relatively short the noise is deflected and scattered by the duct. The overall changes incurred by the duct, however, is small since the first BPF is the dominant source of noise in most cases. It is due to the fact that noise generated by a marine propeller under the non-cavitating condition has a long fundamental wavelength, and the effect of duct is not so important at the far field from the viewpoint of acoustic performance.

ACKNOWLEDGMENTS

This work was supported by Underwater Acoustics Research Center (UARC) and Brain Korea 21 Project in 2001.

REFERENCES

1. D. Ross 1976 *Mechanics of Underwater Noise*. Oxford: Pergamon Press.
2. J. E. Ffowcs Williams and D. L. Hawkings 1969 *Philosophical Transactions of Royal Society Series*, A 264, no. 1151, pp. 321–342. Sound generated by turbulence and surfaces in arbitrary motion.
3. F. Farassat and M. K. Myers 1988 *Journal of Sound and Vibration* **123**(3), 451–460. Extensions of Kirchhoff's formula to radiation from moving surfaces.
4. F. Farrssat and G. P. Succi 1983 *Vertica* **7**(4), 309–320. The prediction of helicopter rotor discrete frequency noise.
5. J. S. Calton 1994 *Marine Propellers and Propulsion*. Oxford: Butterworth-Heinemann.
6. J. E. Kerwin, S. A. Kinnas, J.-T. Lee and W-Z Shin 1987 *Transactions of SNAME*. A surface panel method for the hydrodynamic analysis of ducted propellers.
7. J. E. Kerwin, S. D. Black, T. E. Taylor and C. L. Warren 1997 *Proceedings of the Propeller/Shafting* '97, *Virginia Beach*, *VA*, pp. (21-1)–(21–16). A design procedure for marine vehicles with integrated propulsor.
8. Sangwoo Pyo, Jung-Chun Suh and Kwang Kim 1998 *Proceedings of the* 3*rd International Conference on Hydrodynamics*, *Seoul*, *Korea*. Steady/unsteady analysis of ducted propellers by using a surface panel method.
9. C.-Y. Hsin 1990 *Ph.D. Thesis*, *MIT*, *Department of Ocean Engineering*, 156 pp. Development and analysis of panel methods for propellers in unsteady flow.
10. K.-S. Kim, M.-C. Kim, S.-H. Van J.-C. Suh and J.-T. Lee 1994 *Proceedings of the Propeller/Shafting Symposium* '94, *Virginia Beach*, *VA*, pp. (9-1)–(9–16). A preswirl stator-saving device.
11. M. J. Hughes and S. A. Kinnas 1991 *Proceedings of the Propeller/Shafting Symposium* '91, *Virginia Beach*, *VA*, pp. (15-1)–(15-8). Analysis method for a ducted propeller with pre-swirl stator Blades.

12. M. J. LIGHTHILL 1952 *Proceedings of the Royal Society London, Series* A 211, no. 1107, pp. 564–587. On sound generated aerodynamically, 1. General theory.
13. FARASSAT, F. 1975 *NASA TR R*-451. Theory of noise generation from moving bodies with an application to helicopter rotors.
14. PYO, S. 1995 *Ph.D. thesis, MIT, Department of Ocean Engineering*. Numerical modeling of propeller tip flows with wake sheet roll-up in three dimensions.
15. J. C. SUH, J. T. LEE and S. B. SUH 1992 19*th Symposium on Naval Hydrodynamics, Office of Naval Research*. A bilinear source and doublet distribution over a planar panel, and its application to surface panel method.
16. S. KIRKUP 1998 The Boundary Element Method in Acoustics.
17. R. D. CISKOWSKI and C. A. BREBBIA 1995 *Computational Mechanics Publications, Southampton, Boston*. Boundary element methods in acoustics.
18. A. J. BURTON and G. F. MILLER 1971 *Proceedings of the Royal Society, London, Series A* 323, pp. 201–210. The application of integral equation methods to the numerical solution of some exterior boundary value problems.
19. BYUNGSOK JUNG 2000 *M.S. Thesis, School of Mechanical and Aerospace Engineering, Seoul National University*. The prediction of marine ducted propeller non-cavitation noise using boundary element method.
20. HANSHIN SEOL, BYUNGSOK JUNG and SOOGAB LEE 2000 *Proceedings of the* 1*st National Congress on Fluids Engineering, Muju, Korea*, pp. 255–258. Prediction of non-cavitating underwater propeller noise.
21. HANSHIN SEOL, BYUNGSOK JUNG, CHEOLUNG CHEONG and SOOGAB LEE 1999 *Proceedings of Acoustical Society of Korea* '1999, Seoul, Korea. A numerical study on the prediction of marine propeller non-cavitation noise.
22. HANSHIN SEOL 2001 *M.S. Thesis, School of Mechanical and Aerospace Engineering, Seoul National University*. The prediction of non-cavitating underwater propeller noise.

APPENDIX: NOMENCLATURE

Time-domain acoustic analogy

c_0	speed of sound
$f(\mathbf{x}, t) = 0$	equation of blade surface
l_i	local force per unit area on fluid in direction i
M	Mach number
M_r	Mach number in radiation direction
$\hat{n}$	unit outward normal vector to surface $f = 0$
$p'(\mathbf{x}, t)$	acoustic pressure
r	length of radiation vector, $\lvert\mathbf{x} - \mathbf{y}\rvert$
$\mathbf{r}$	radiation vector, $\lvert\mathbf{x} - \mathbf{y}\rvert$
$\hat{r}$	unit radiation vector, $\mathbf{r}/r$
t	observer time
$\hat{t}$	unit tangent vector to surface $f = 0$
v_n	local normal velocity of blade surface
$\mathbf{v}$	local velocity of blade surface
$\mathbf{x}$	observer position in frame
$\mathbf{x}_{OBS}$	observer location
$\mathbf{y}$	source position
$\mathbf{y}_0(t)$	position vector from origin of ground-fixed frame to moving frame
τ	source time
ret	evaluated at retarded or emission time Boundary Element Method

Boundary element method

p_i'	incident acoustic pressure in ground-fixed frame
p_s'	scattered acoustic pressure in ground-fixed frame
p_t'	total acoustic pressure in ground-fixed frame
u_n	normal component of acoustic velocity in ground fixed-frame

P'_i	incident acoustic pressure in moving frame
P'_s	scattered acoustic pressure in moving frame
P'_t	total acoustic pressure in moving frame
U_N	normal component of acoustic velocity in moving frame
Z	axial co-ordinate of moving frame
r_{max}	maximum propeller radius
V_F	forward speed of duct
M_F	$= V_F/c$, forward Mach number
β	$\sqrt{1 - M_F^2}$, stretching parameter
N_B	number of blades
M_{TIP}	tip Mach number
Ω	shaft angular velocity
m	circumferential mode number
k	non-dimensional characteristic wave number
κ	$= k/\beta$, stretched non-dimensional characteristic wave number
k_z	axial wave number
J_m	mth order Bessel function of first kind
v_m	first zero of J'_m
ζ	acoustic impedance of duct surface